

Quantum Depletion of Superconductivity in 3D Diamond Nanowires

Gufei Zhang,* Simon Collienne, Ramiz Zulkharnay, Xiaoxing Ke, Liwang Liu, Songyu Li, Sen Zhang, Yongzhe Zhang, Yejun Li, N. Asger Mortensen, Victor V. Moshchalkov, Jiaqi Zhu, Alejandro V. Silhanek,* and Paul W. May*

Superconducting nanowires underpin the development of a variety of highly advanced quantum devices such as single-photon detectors and quantum circuits. In 1D superconducting nanowires, topological fluctuations of the superconducting order parameter, known as phase slips, severely influence the electrical transport. In 3D systems, however, phase-slip events are generally considered to be insignificant. Here, details on the observation of a reentrant resistive state in 3D superconducting diamond nanowires (DNWs) are reported. This exotic resistive state alters the trend of the superconducting transition with an abrupt change of the temperature and magnetic-field coefficients of resistivity and the current coefficient of voltage. This reentrant resistive state is interpreted as being a result of quantum phase slips in the bamboo-like DNWs consisting of multiple sequential grain-boundary-grain junctions. The results provide the first evidence that quantum phase slips can also play a crucial role in determining the electrical transport properties of 3D superconducting nanowires.

1. Introduction

Traditional information technologies based on conventional electronic materials are rapidly approaching their limit. Advanced materials and nanotechnology are required for the development of novel devices of reduced footprint but with simultaneously enhanced performance and reduced energy dissipation. As a wide-band-gap semiconductor, diamond has drawn a large amount of attention for its superior performance in thermionics,^[1] power and logic electronics,^[2–4] and electromechanics.^[5] Apart from benefitting the semiconductor industry, diamond has also opened new perspectives in quantum information technology by being the host material of emergent quantum phenomena. For example, the spin states of negatively charged color

G. Zhang, S. Zhang, J. Zhu
National Key Laboratory of Science and Technology on Advanced Composites in Special Environments
Harbin Institute of Technology
Harbin 150080, China
E-mail: sp3.zhang@gmail.com

G. Zhang, S. Zhang, J. Zhu
Zhengzhou Research Institute
Harbin Institute of Technology
Zhengzhou 450000, China

S. Collienne, A. V. Silhanek
Q-MAT
Experimental Physics of Nanostructured Materials (EPNM)
University of Liege (ULiege)
Department of Physics B5a
Liège 4000, Belgium
E-mail: asilhanek@uliege.be

R. Zulkharnay, P. W. May
School of Chemistry
University of Bristol
Bristol BS8 1TS, UK
E-mail: paul.may@bristol.ac.uk

X. Ke, S. Li, Y. Zhang
Faculty of Materials & Manufacturing and Faculty of Information Technology
Beijing University of Technology
Beijing 100124, China

L. Liu, V. V. Moshchalkov
Department of Physics and Astronomy
KU Leuven
Heverlee B-3001, Belgium

Y. Li
School of Physics & Electronics and School of Materials Science & Engineering
Central South University
Changsha 410083, China

N. A. Mortensen
POLIMA—Center for Polariton-Driven Light-Matter Interactions and Danish Institute for Advanced Study
University of Southern Denmark
Campusvej 55, Odense M DK-5230, Denmark

 The ORCID identification number(s) for the author(s) of this article can be found under <https://doi.org/10.1002/qute.202400476>

© 2024 The Author(s). Advanced Quantum Technologies published by Wiley-VCH GmbH. This is an open access article under the terms of the [Creative Commons Attribution](https://creativecommons.org/licenses/by/4.0/) License, which permits use, distribution and reproduction in any medium, provided the original work is properly cited.

DOI: 10.1002/qute.202400476

centers in diamond have demonstrated their potential in quantum computing,^[6] and the discovery of Yu-Shiba-Rusinov bands in ferromagnetic superconducting diamond thin films has paved a path toward the engineering of topologically protected qubits.^[7,8]

Superconducting boron-doped diamond has drawn considerable attention due to its nature of being a doped insulator.^[9,10] Research on boron-doped diamond has revealed that as the boron concentration reaches $\approx 5 \times 10^{20} \text{ cm}^{-3}$, an insulator-metal transition takes place along with the emergence of superconductivity in this material.^[11] Due to their minute Ginzburg–Landau coherence length, $\xi < 15 \text{ nm}$,^[12] superconducting diamond is mostly located in the 3-dimensional (3D) regime. Moreover, granular diamond has been demonstrated to be the host of a series of quantum confinement phenomena, e.g., the anomalous resistance peak prior to the superconducting transition,^[13] strong granularity-correlated modulations of the superconducting order parameter,^[14] and anomalous superconducting anisotropy.^[15]

When narrowing a superconductor to the 1D limit by reducing its width and thickness below ξ , its transport properties can change dramatically due to phase-slip events. A phase-slip event corresponds to a local suppression of the amplitude of the superconducting order parameter along with a change of the phase by 2π .^[16] The two local minima of the Ginzburg–Landau free energy corresponding to 0 and 2π are separated by an energy barrier that can be overcome at relatively high temperatures, leading to thermally activated phase slip (TAPS). At low temperatures and even down to zero temperature, a transition from one state to the other can still take place via tunneling through the barrier, which gives rise to a quantum phase slip (QPS).^[16]

Investigations of the activation mechanisms of phase slips are of fundamental importance to advancing the development of quantum technologies. A crossover from TAPS to QPS has been found in MoGe nanowires, followed by its theoretical demonstration for 1D superconducting nanowires in general.^[17,18] Such a crossover has also been observed in nanowires made from In,^[19] Nb,^[20] Zn,^[21] Al,^[22] and NbN,^[23] where a TAPS-correlated resistance drop converts into a QPS-correlated resistive tail extending toward zero temperature. In addition, research efforts have also been devoted to suppressing phase slips in Al nanowires with the aim of using such wires to sustain phase coherence in superconducting quantum circuits.^[24] It is also noteworthy that time-resolved transport measurements have been demonstrated to be feasible for the temporal detection of phase slips.^[25]

Here, we report on the observation of a reentrant resistive state in 3D superconducting diamond nanowires (DNWs) fabricated from heavily boron-doped polycrystalline diamond thin films (DTFs). In contrast to the conventional superconducting transition in the starting materials, the superconducting transition in the DNWs is interrupted by the appearance of a resistive state which bears a close resemblance to the QPS-correlated resistive tail observed in 1D superconducting nanowires. Consistent with its fingerprints in the temperature dependence of resistivity, $\rho(T)$, the reentrant resistive state correspondingly manifests itself as a peak in the magnetic-field dependence of resistivity, $\rho(H)$, and the current dependence of voltage, $V(I)$. Taking into account the bamboo-like structure of the DNWs, where the half-micron-sized superconducting diamond crystallites are separated by high-resistance grain boundaries, we conceptually

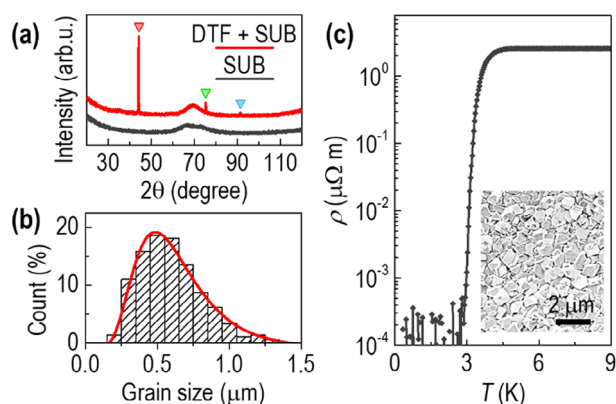


Figure 1. Heavily boron-doped polycrystalline diamond thin films (DTFs) grown on SiO_2/Si substrates (SUB). (a) X-ray diffraction spectra. The diffraction peaks, (111) (red triangle), (220) (green triangle), and (311) (blue triangle), are indicative of the polycrystalline nature of the DTFs. The broad diffusive peak at $\approx 70^\circ$ originates from the substrate. (b) Grain-size analysis based on the SEM image inset in (c). The grain size statistics (bar chart) follow a lognormal distribution (red curve). (c) The DTFs exhibit a rather broad resistive superconducting transition at low temperatures, due to the electrical percolation characteristics of this granular disordered system.^[26]

treat them as 1D chains of weak links, and interpret their reentrant resistive state as being a result of phase-slip events induced primarily by quantum tunneling in the framework of the Giordano model.^[19] Our findings suggest that the weak links at the grain boundaries in a 3D superconducting nanowire could facilitate the movement of magnetic flux quanta across the DNWs, thus promoting phase-slip events.

2. Results and Discussion

Heavily boron-doped polycrystalline DTFs with a film thickness of about 850 nm, a mean grain size of $\approx 570 \text{ nm}$, and a boron concentration of $\approx 3 \times 10^{21} \text{ cm}^{-3}$ are used as the starting material to fabricate our samples (see Figure 1).^[26] These DTFs are deposited on SiO_2/Si substrates using chemical vapor deposition (CVD) (see Experimental Section). As shown in Figure 1c, the DTFs exhibit a resistive superconducting transition with the onset and offset critical temperatures, T_c^{onset} and T_c^{offset} , being 4.5 and 2.7 K, respectively.^[26] Granular disordered superconductors, such as our starting material, generally show a resistive superconducting transition significantly broader than those of disorder-free systems. This is because, in the presence of granular disorder, percolation paths need to be established via intergrain coupling such that Cooper pairs can flow through the system, allowing the emergence of the zero-resistance state.^[27]

As an ensemble of interconnected diamond grains with different crystallographic orientations, a polycrystalline DTF shows large variations in the local height, which is detrimental to nanolithography. To mitigate this challenge, we fabricated the DNWs through a two-stage process (see Figure 2a): 1) The DTFs were patterned into micro-crosses by the combined use of electron-beam lithography (EBL), electron-beam evaporation (EBE), and reactive ion etching (RIE); 2) The central parts of the diamond micro-crosses were then patterned into U-shaped DNWs via

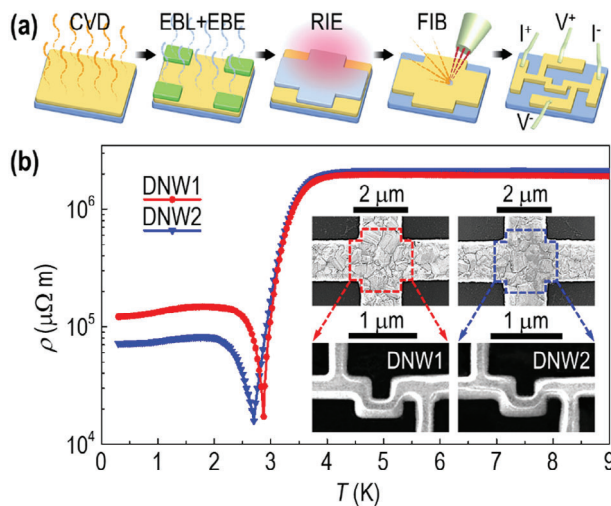


Figure 2. Reentrant resistive state in superconducting diamond nanowires (DNWs) fabricated from heavily boron-doped polycrystalline diamond thin films. (a) Schematic illustration of the fabrication process. The diamond thin films (yellow) grown on substrates (blue) via chemical vapor deposition (CVD), were first patterned into micro-crosses by using electron-beam lithography (EBL) combined with electron-beam evaporation (EBE) and reactive ion etching (RIE). The micro-crosses were then patterned into DNWs through focused ion beam (FIB) milling. Green: Photoresist. Grey: Al mask. Pink: Oxygen plasma. Dark red: Ga ion beam. (b) The resistive superconducting transition in the DNWs is interrupted by the uprise of an exotic resistive state extending toward zero temperature, giving rise to an anomalous dip in the temperature dependence of resistivity, $\rho(T)$. Inset: SEM images of DNW1, DNW2, and the two micro-crosses from which the DNWs were manufactured. During the FIB milling, despite vacuum pumping, a thin layer of high-resistance amorphous carbon was redeposited onto the surface of the DNWs, making the grain boundaries invisible.

focused ion beam (FIB) milling (see Experimental Section). The U-shaped structure facilitates length extension of the DNWs in a limited space, allowing for the incorporation of multiple grain-boundary-grain junctions in the nanowires. The DNWs each have two pairs of electrical leads attached for four-probe electrical transport measurements (see Experimental Section), where the pair of leads aligned on the same line was used to send current, and the other pair was used to measure the voltage drop across a DNW (see the inset to Figure 2b). The DNWs and their electrical leads were made from the same material. As a result of the FIB milling, the DNWs have a trapezoidal cross-section with its height being the film thickness of the starting material and its upper and bottom edges being ≈ 170 and 330 nm, respectively. Here, we present the data of two DNWs (labeled DNW1 and DNW2), fabricated from the same DTF film and under identical conditions, to demonstrate the repeatability of our findings.

Below the T_c^{onset} of the starting material, DNW1 and DNW2 show a resistivity drop nearly identical to that of the unpatterned DTF (see Figure 2b). As the temperature decreases further, the resistivity drop in the DNWs is reversed, giving rise to an anomalous dip at ≈ 2.9 K in DNW1 and 2.7 K in DNW2. Below the dip temperature, T_{dip} , the $\rho(T)$ increases to a maximum at ≈ 1.8 K and then evolves into a slowly decreasing resistive tail extending toward zero temperature. Note that the residual resistivity of the DNWs is significantly larger than that of the starting material,

and no zero-resistance state is observed in the DNWs. This is because when patterning a DTF into DNWs, the percolation paths in the DTF are truncated, and the charge carriers have no other choice but to embark on the only path composed of the remaining grain-boundary-grain junctions in the DNWs.

To gain further insight into the reentrant resistive state below T_{dip} , the $\rho(H)$ of the DNWs were measured at different temperatures by applying magnetic fields in the out-of-plane direction. As shown in Figure 3, consistent with their $\rho(T)$ behavior, the DNWs demonstrate the reentrant resistive state as a finite resistivity peak superimposed on the superconducting transition in $\rho(H)$. As the temperature increases, this resistivity peak narrows down and fades out when approaching T_{dip} . Such a resistivity peak, previously reported for 1D superconducting nanowires made from Zn,^[21] Pb,^[28] Nb,^[29] MoGe,^[29] and Al,^[30] is often referred to as “negative magnetoresistance (NMR)” in accordance with its negative magnetic-field coefficient.

Such NMR has been recognized as a fingerprint of QPS-dominated depletion of superconductivity, yet its origin still remains elusive. The following two alternative models have been widely employed to explain the NMR features observed in various superconducting nanowires:

Model (1): Phase slips take place as periodic oscillations of the superconducting order parameter in time at the so-called phase-slip centers (PSCs) which are normally induced by local inhomogeneities in a nanowire.^[31] The fast oscillations of the superconducting order parameter within a region of size $\sim \xi$ represents a time-periodic depletion of the local superconductivity with the consequent proliferation of single quasiparticles. These quasiparticles diffuse away and recombine into Cooper pairs within a region of a much larger size λ_Q (known as the charge imbalance length) around the PSCs. In the low-field regime, the decrease of λ_Q upon the increase of applied magnetic fields can lead to an enhancement of the critical current, which will, in turn, result in the suppression of the rate of phase slips and thus the decrease of resistance.^[21,31–33]

Model (2): In many cases, a superconducting nanowire and its electrical leads are manufactured from the same superconducting thin film. In contrast to the nanowire of a reduced dimensionality, the larger-sized superconducting leads have a lower critical magnetic field. Upon the increase of the applied magnetic fields, the superconductivity in the electrical leads attached to the nanowire will be suppressed, leading to an increase of the normal component of the current, I_N , and thus a decrease of the superconducting component of the current, I_S , flowing through the nanowire. Because I_S is the driving force of phase-slip events, its decrease will result in the suppression of the rate of phase slips and thus the decrease of resistance.^[32,34]

Despite their success in explaining some experimental observations, these two models appear to have their own limitations. For example, according to Model (1), the NMR feature is supposed to be present in a superconducting nanowire of arbitrary length, while experimental studies have revealed that the emergence of the NMR could be dependent on the length of the nanowire.^[34] In contrast, for Model (2), the onset magnetic field of the NMR in a nanowire should coincide with the upper critical magnetic field, H_{c2} , of the superconducting leads,^[30] which is nearly identical to the H_{c2} of the film from which the leads are fabricated (unlike the nanowire with a reduced dimensionality,

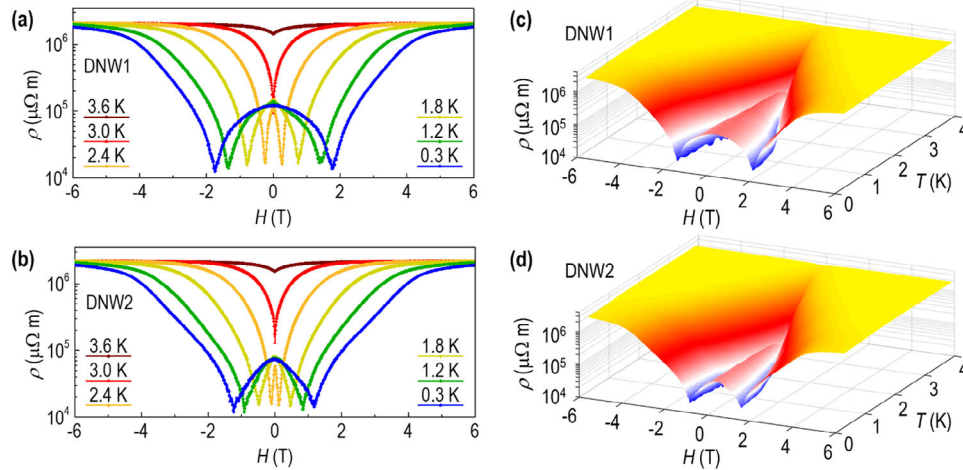


Figure 3. Negative magnetoresistance (NMR) in the diamond nanowires. (a),(b) The reentrant resistive state manifests itself as an NMR peak superimposed on the resistive superconducting transition in the magnetic-field dependence of resistivity, $\rho(H)$. (c),(d) Temperature-induced evolution of the NMR peak. As the temperature increases, the NMR peak narrows down and fades out at the dip temperature in $\rho(T)$ (see Figure 2b).

the larger-sized leads are normally of the same dimensionality as the superconducting film). This is clearly not the case with the DNWs investigated in this work, where the onset magnetic field of the NMR, H_{dip} , deviates distinctly from the H_{c2} of the DTF (see Figure 4).

Figure 4 shows the phase diagram of the DNWs. The $H_{c2}-T$ phase boundaries of the DNWs are extracted from their $\rho(H)$ dependences, in practice by setting the criterion at 95% of the normal-state resistance, and the $H_{\text{dip}}-T$ phase boundaries are obtained by tracking the shift of the dip field, H_{dip} (see the inset to Figure 4). The $H_{c2}-T$ phase boundary of the DTF, constructed with the same approach as for the DNWs,^[26] is added to the plots for comparison. In contrast to the DTF with a

quadratic $H_{c2}-T$ phase boundary, the DNWs demonstrate linear $H_{c2}-T$ dependences. By extrapolating these $H_{c2}-T$ dependences down to zero temperature, ξ is determined to be 8.6 nm for the DTF, 6.6 nm for DNW1, and 6.5 nm for DNW2, according to the relation $\xi = [\Phi_0/2\pi H(0 \text{ K})]^{0.5}$ with Φ_0 being the magnetic flux quantum.^[35]

The reduced ξ of the DNWs is indicative of an enhanced confinement of Cooper pairs. Quantum confinement effects are most pronounced in low-dimensional systems with at least one of the dimensions being smaller than a characteristic length (e.g., ξ). Although the DNWs are located deeply in the 3D regime due to their relatively large dimensions in contrast to the minute ξ , the grain boundaries can promote confinement effects. When patterning a polycrystalline DTF into a nanowire with a width smaller than the mean grain size, such as DNW1 and DNW2, the grain boundaries traversing across the nanowire will divide it into several parts, giving rise to a wire morphology resembling that of a bamboo rod. In this case, the grain boundaries become more influential in determining the electrical transport, because unlike in a DTF, the Cooper pairs in a DNW have no alternative percolation paths but have instead a chain of barriers associated with the cross-sectional grain boundaries to overcome in sequence.

Moreover, as mentioned above, based on the distinct separation between the $H_{\text{dip}}-T$ phase boundaries of the DNWs and the $H_{c2}-T$ phase boundary of the DTF (see Figure 4), Model (2) can be excluded as the cause of the NMR in our DNWs, leaving Model (1), the reduction of λ_Q , to be the most probable mechanism for the explanation of our observations.

Consistent with its presence in the $\rho(T)$ and $\rho(H)$, the reentrant resistive state also reveals its existence in the $V(I)$ measurements. As shown in Figure 5, at low temperatures, the reentrant resistive state emerges as a low-current peak which shrinks upon the increase of temperature. Similarly to the $\rho(H)$ peak, this $V(I)$ peak also fades out when the temperature approaches T_{dip} .

Apart from the fact that the $V(I)$ peak has been rarely reported for other systems, the $V(I)$ dependences of the DNWs also

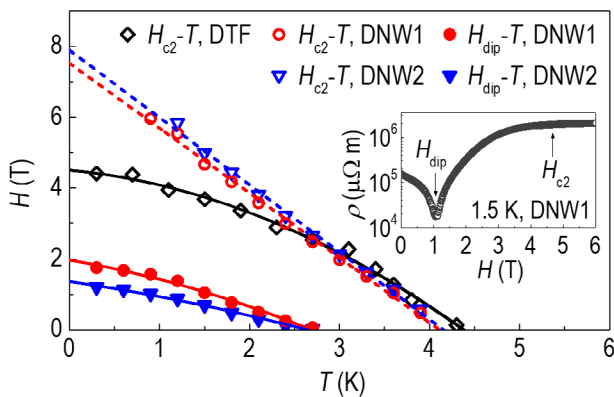


Figure 4. Magnetic field vs temperature phase diagram of the diamond nanowires. In contrast to the DTF, the DNWs show a linear temperature dependence of the upper critical magnetic field, $H_{c2}-T$. By tracking the temperature-induced shift of the dip field, H_{dip} (see the inset and Figure 3), the $H_{\text{dip}}-T$ phase boundaries are constructed for the DNWs. Note that the $H_{c2}-T$ phase boundary of the DTF lies well above the $H_{\text{dip}}-T$ phase boundaries of the DNWs, indicating that the NMR peak in Figure 3 cannot be attributed to the suppression of the superconductivity in electrical leads. Dashed lines: Linear fits. Solid curves: Quadratic fits.

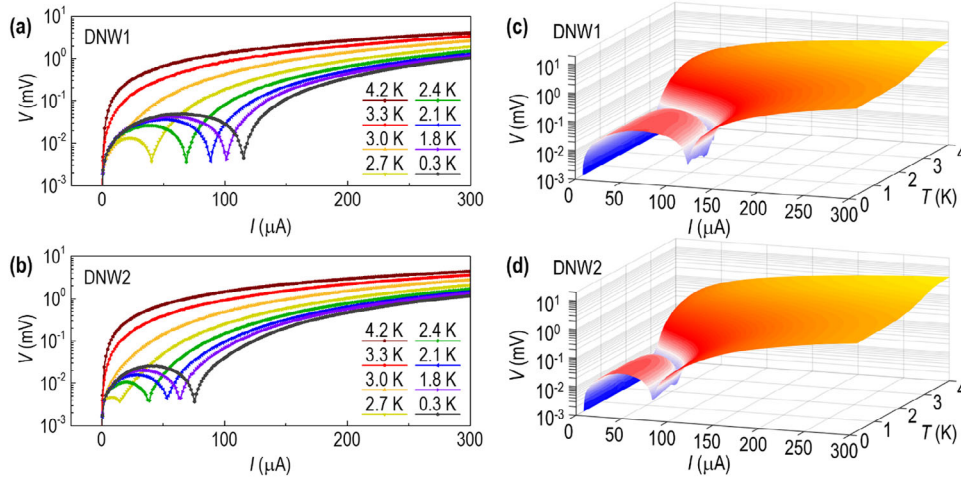


Figure 5. Appearance of the reentrant resistive state in the current dependence of voltage, $V(I)$, of the diamond nanowires. (a),(b) The reentrant resistive state appears as a $V(I)$ peak in the low-current range. (c),(d) Temperature-induced evolution of the $V(I)$ peak. As the temperature increases, the $V(I)$ peak shrinks and fades out at the dip temperature in $\rho(T)$ (see Figure 2b).

differ from those of 1D superconducting nanowires due to the absence of discrete voltage jumps. The $V(I)$ characteristics of 1D superconducting nanowires often feature a stepwise structure with discrete voltage jumps which translate into resistive steps, and the linear extrapolations of these resistive steps converge to a non-zero time-averaged supercurrent at zero voltage.^[23,36] Such resistive steps can be explained in the framework of Model (1). Because $\lambda_Q \gg \xi$, the region of size ξ over which the fast oscillations of the superconducting order parameter take place can be neglected, and a phase slip can be viewed as a time-independent (stationary) process. In such a model, each resistive step can be attributed to the formation of a new PSC.^[31]

The formation of PSCs can be confirmed by the presence of resistive steps in $V(I)$, while the absence of such steps cannot be used as an argument to affirm the nonexistence of PSCs. It has been demonstrated theoretically that in the presence of “defects” (defined as regions over which the local superconducting transition temperature and superconducting order parameter are suppressed), the amplitude of voltage jumps decreases as the “strength” of the defects increases,^[31] making it possible for the resistive steps to disappear. The high-resistance grain boundaries in our DNWs can be naturally regarded as correlated defects. Another possible cause of the absence of voltage jumps in $V(I)$ could be averaging effects from the grain-boundary-grain junctions with different geometries. In the granular DNWs, the self-assembled junctions have neither a uniform geometry nor an even distribution.

Figure 6 shows the phase diagram of the reentrant resistive state in I - T space. By tracking the onset current of the reentrant resistive state, I_{dip} , at different temperatures (see Figure 5 and the inset to Figure 6), we build up the I_{dip} - T phase boundaries of the DNWs. As the temperature decreases, the DNWs show a pronounced increase of I_{dip} , which tends to saturate at low temperatures. Close to T_{dip} , the increase of I_{dip} is described well by an empirical power law as in

$$I_{\text{dip}} = I_0 \left(1 - \frac{T}{T_{\text{dip}}} \right)^\eta \quad (1)$$

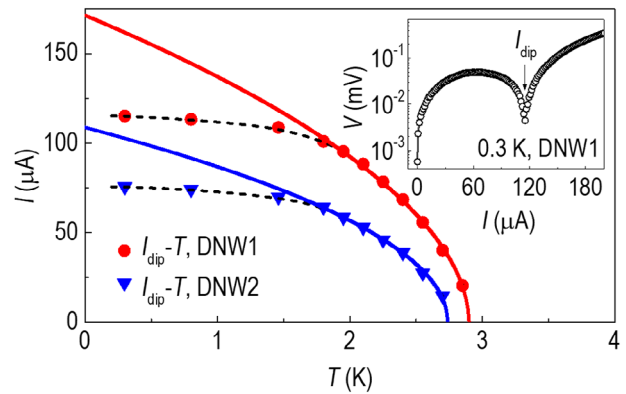


Figure 6. Current-temperature phase diagram of the diamond nanowires. By tracking the temperature-induced shift of the dip current, I_{dip} (see the inset and Figure 5), the I_{dip} - T phase boundaries are built up for the DNWs. Solid curves: Fits by an empirical power law (Equation 1). Dashed curves: A guide to the eye.

Through fitting, an identical exponent of $\eta = 0.5$ was obtained for DNW1 and DNW2, and the prefactor, I_0 , was determined to be 171 μA for DNW1 and 109 μA for DNW2.

To elucidate the influence of the device geometry and grain boundaries on the electrical transport in the DNWs, we start off by neglecting possible quantum effects and model instead their classical voltage and current distributions in the normal state, using a finite-element implementation of the charge-transport problem (Comsol Multiphysics).^[37] By referring to the scanning electron microscopy (SEM) images of the DNWs and taking into account their trapezoidal cross-section, we created the device layout for modeling, where arbitrary grain boundaries with a thickness of $d = 5$ nm are arranged in accordance with the mean grain size of the starting material (see Figure 7a). Because the grain boundaries are far more resistive than the diamond grains, their conductivity is for illustrative purposes set to be $\sigma_b = \sigma_g/100$ with σ_g being the conductivity of the grains. A uniform current density, J_0 , is fed through the left electrical lead while a ground

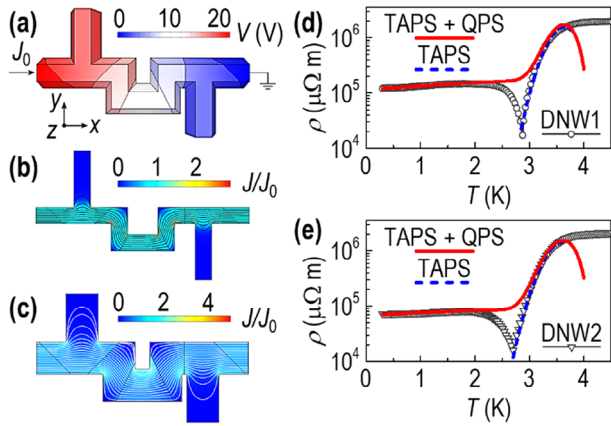


Figure 7. Modeling of the electrical transport in the diamond nanowires. (a) Voltage distribution in the normal state. The device geometry is taken from the SEM images of the DNWs which have a trapezoidal cross section. Due to the contact impedance at the grain boundaries traversing across the nanowire (black lines), the modeled device demonstrates significant voltage drops along its length. (b),(c) Current distribution in the normal state. In contrast to the top surface (b), the bottom surface (c) exhibits a more pronounced current crowding. (d),(e) Modeling of the low-temperature behavior of the DNWs in the framework of thermally activated and quantum phase slips. Dashed blue curves: Fits by Equation (2). Solid red curves: Fits by Equation (4).

condition is imposed on the right lead. The voltage, V , is obtained by solving the Poisson equation, $\nabla \cdot \mathbf{J} = 0$, where $\mathbf{J} = \sigma_{\text{g}} \mathbf{E}$ is the current density in A m^{-2} with $\mathbf{E} = -\nabla V$ being the electric field in V m^{-1} .

Figure 7a shows the resulting voltage distribution in the modeled device. In contrast to the grains with a rather homogeneous potential, the grain boundaries host significant voltage drops. The voltage drop across a grain boundary, arising from the contact impedance between the grains, is $\Delta V = \mathbf{n} \cdot \mathbf{J} d / \sigma_{\text{b}}$, where \mathbf{n} is the unit vector normal to the boundary. Figure 7b,c illustrates the relative current density, J / J_0 , at the top and bottom surfaces of the modeled device, respectively. In contrast to the top surface, the bottom surface demonstrates a more pronounced current crowding, suggesting that vortex nucleation may be more favorable at the bottom of the device.

Our findings in the DNWs, such as the resistive tail in the $\rho(T)$ and its associated $\rho(H)$ and $V(I)$ peaks, all suggest a phase-slip-dominated depletion of the superconductivity below T_{dip} . Because no theoretical model has yet been put forward for quantitative analysis of superconducting nanowires in 3D, the theoretical models established for 1D systems are adapted to shed light on the activation mechanisms of the phase slips in our DNWs.

In the case of a 1D superconducting nanowire, TAPS events taking place close to the superconducting transition temperature, T_{c} , will lead to a broadening of its $\rho(T)$ dependence, which can be well described by the Lamber-Ambegaokar-McCumber-Halperin (LAMH) theory,^[38,39]

$$\rho_{\text{TAPS}} = \frac{\pi \hbar^2 \Omega_{\text{TAPS}}(T)}{2e^2 k_{\text{B}} T} \exp \left\{ -\frac{\Delta F(T)}{k_{\text{B}} T} \right\} \quad (2)$$

where $\Omega_{\text{TAPS}}(T) = [L / \xi(T)] [1 / \tau_{\text{GL}}] [\Delta F(T) / (k_{\text{B}} T)]^{0.5}$ is the attempt frequency, $\Delta F(T) = [4\sqrt{2} / (3\mu_0)] H_{\text{c}2}(T)^2 A \xi(T)$ is the

Table 1. TAPS and QPS adjusting parameters used to model the low-temperature behavior of the DNWs.

	L (nm)	A (10^{-3} nm^2)	B (10^{-3})	C
Nanowire				
DNW1	0.37 ± 0.03	3.4 ± 0.15	10.3 ± 0.3	0.22 ± 0.01
DNW2	0.28 ± 0.01	2.7 ± 0.1	6.1 ± 0.3	0.22 ± 0.01

condensation energy barrier, $\tau_{\text{GL}} = \pi \hbar / [8k_{\text{B}}(T_{\text{c}} - T)]$ is the characteristic Ginzburg-Landau time, k_{B} is the Boltzmann constant, \hbar is the reduced Planck constant, L is the length of the nanowire, and A is the cross-sectional area of the wire.

At lower temperatures, the reduction of $\Delta F(T)$ makes it more likely for QPS to occur, as described by Giordano's model,^[19,40]

$$\rho_{\text{QPS}} = B \frac{\pi \hbar^2 \Omega_{\text{QPS}}(T)}{2e^2 (\hbar / \tau_{\text{GL}})} \exp \left\{ -C \frac{\Delta F(T)}{\hbar / \tau_{\text{GL}}} \right\} \quad (3)$$

where $\Omega_{\text{QPS}}(T) = [L / \xi(T)] [1 / \tau_{\text{GL}}] [\Delta F(T) / (\hbar / \tau_{\text{GL}})]^{0.5}$ is the new attempt frequency, and B and C are two adjustable phenomenological parameters.

As shown in Figure 7d,e, the LAHM theory alone can only provide a fairly good description of the resistive superconducting transition above T_{dip} , whereas the series combination of the two theories,

$$\rho_{\text{total}} = \rho_{\text{TAPS}} + \rho_{\text{QPS}} \quad (4)$$

enables the modeling of our experimental data over a much wider temperature range including the resistive tail at low temperatures. To facilitate the fitting, L and A are adopted as adjusting parameters as well as B and C (see Table 1). The significant mismatch between the actual dimensions of the DNWs and their L and A values obtained from fitting may be due to our application of the LAHM and Giordano models to a system located deeply in the 3D regime. Note that Equation (4) is unable to capture the $\rho(T)$ dip observed in our 3D DNWs, even though it has managed to reproduce the $\rho(T)$ of a variety of 1D superconducting nanowires where the crossover from TAPS to QPS manifests itself as a kink.^[17,19,20,22,23] It is also noteworthy that the downturn of the fitted curves at $T \sim T_{\text{c}}$ arises from an artifact of the LAHM theory, i.e., when T approaches T_{c} , τ_{GL} increases indefinitely, and $\Omega_{\text{TAPS}}(T)$ tends to zero (see Equation 2).^[41]

3. Conclusion

To conclude, we have found a reentrant resistive state in superconducting polycrystalline DNWs. This exotic resistive state consistently demonstrates its existence in the $\rho(T)$, $\rho(H)$, and $V(I)$ dependences of the 3D DNWs by counteracting the superconducting transition. Based on its resemblance to the behavior of 1D superconducting nanowires, we interpret the reentrant resistive state as being a result of the phase-slip-correlated depletion of superconductivity in the granular DNWs. Our experimental data and theoretical analyses suggest that the emergence of the reentrant resistive state can be driven by QPS. The absence of resistive steps in the $V(I)$ dependence of the NDWs, however, remains elusive and calls for follow-up studies. Our results, obtained from

granular DNWs in the 3D regime, can add to the elucidation of the hitherto concealed mechanisms of phase-slip events. Our findings indicate that in the presence of granular disorder, even a 3D superconducting nanowire can be severely influenced by phase-slip events, thus making the system unsuitable for use as a building block to engineer quantum circuits. With the nanowires being a technologically feasible platform, our findings could foster the development of diamond-based single-photon detectors.

4. Experimental Section

Growth of the Starting Material: The heavily boron-doped diamond thin films were deposited using hot filament CVD onto undoped Si (100) substrates onto which had been grown a thin (300 nm) of SiO₂. This insulating oxide layer was to ensure that all measured electrical signals originated from the DTF and not from the Si substrate. These substrates were cleaned in acetone and then isopropanol for 15 min each and finally rinsed with deionized water in an ultrasonic bath. To enable diamond deposition, the substrates were then seeded with nanodiamond particles (average particle size $\approx 3.3 \pm 0.6$ nm, NanoCarbon Research Institute Ltd., Japan) using an electrospray deposition technique.^[42] The CVD process used a gas mixture containing 1% CH₄ in H₂ plus B₂H₆ (at a B:C ratio of 8750 ppm). Resistively heated tantalum filaments (>2000 °C) thermally decomposed the feedstock gases into reactive atoms and radicals at a pressure of 20 torr, initiating the deposition of a continuous boron-doped diamond layer onto the substrate, which was situated 3 mm below the filaments at a temperature ≈ 800 °C. Nanocrystalline DTFs of thickness ~ 500 nm resulted following a deposition time of 1 h. The boron concentration of the DTFs was determined to be about 3.3×10^{21} cm⁻³ through Hall effect measurements previously calibrated with secondary ion mass spectrometry (SIMS). The mean grain size of the DTFs was obtained by analyzing SEM images with *ImageJ* software.

Fabrication of the DNWs: These were fabricated in two steps, first, the DTFs were patterned into micron-scale crosses by traditional photolithography and dry etching, and then these patterns were refined into the final higher-resolution DNWs using FIB milling (see Figure 2a).

To fabricate the diamond micro-crosses, an EBL facility (ELS-7500EX) with an acceleration voltage of 50 kV and an electron-beam current of ≈ 1 nA was used to define the micro-cross patterns on the surface of the DTF. After developing the photoresist, a 100-nm-thick Al layer was evaporated onto the patterned DTFs using EBE (base pressure of $\approx 10^{-5}$ Pa). This Al layer was required to act as a non-erodible mask because the O₂-based process used to dry-etch diamond also etches organic photoresist. RIE was then performed in a 13.56 MHz inductively coupled plasma reactor (ULVAC CE300I) in an O₂ atmosphere (flow rate 90 sccm) at 0.5 Pa. The RF power was split between 800 W on the chamber to sustain the plasma and 20 W applied to the substrate electrode to create a DC bias and ensure anisotropic etching. The RIE process was automatically stopped once the Si substrate was reached, as confirmed by a profilometer measuring the etching depth. The Al mask was then chemically removed in a solution of trimethylamine and the samples were ultrasonically cleaned in deionized water. The contact pads were then fabricated by depositing a bilayer of Ti (10 nm) / Au (100 nm) using EBE, as before, and a standard lift-off process to define the pattern. Finally, the samples were cleaned ultrasonically in acetone, methanol, and then in deionized water.

Following the microfabrication of the micro-crosses, a FIB system (FEI Helios FIB/SEM DualBeam using a 30 kV Ga-ion beam) was used to refine these patterns into DNWs. The patterning was performed using a two-step procedure: a) rough patterning with a beam current of 0.43 nA for the preparation of trenches; b) fine trimming using a beam current of 0.23 nA–80 pA to mitigate any beam damage to the final diamond nanowires and to ensure the correct linewidth. A side-effect of the ion milling was that a thin layer of high-resistance amorphous carbon was redeposited onto the surface of the DNWs. This layer blurs out the height difference between the diamond crystallites and covers the grain boundaries, making the grain boundaries invisible on SEM images (Figure 2b).

Electrical Transport Measurements: A ³He/⁴He cryostat equipped with a d.c. magnet was used to measure the electrical transport properties of the samples. All measurements were carried out with the four-terminal approach by sending a low-frequency a.c. current through the samples and probing the voltage drop with a lock-in amplifier. In contrast to 1D superconducting nanowires, the DNWs in 3D have a quite large critical current well above 500 μ A. To assure the sample safety and to maintain temperature stability, the excitation current sent through the DNWs was not increased beyond 500 μ A in the $V(I)$ measurements.

Acknowledgements

This work was supported by the Harbin Institute of Technology Ideation Fund (HIT.DZJJ.2023041), the Major Science and Technology Special Project of Zhengzhou (2021KJZX0062), the Major Science and Technology Special Project of Henan Province (221100230300), the Fonds de la Recherche Scientifique – FNRS under the grants Excellence of Science (EOS) project O.0028.22, the Bolashak International Scholarship programme of the Republic of Kazakhstan, the National Natural Science Foundation of China (12074017, 12274010 and 11904411), and the FWO (Research Foundation-Flanders) (12V4422N).

Conflict of Interest

The authors declare no conflict of interest.

Data Availability Statement

The data that support the findings of this study are available from the corresponding author upon reasonable request.

Keywords

diamond nanowires, grain-boundary-grain junctions, negative magnetoresistance, quantum phase slips, reentrant resistive state

Received: September 25, 2024

Revised: November 27, 2024

Published online:

- [1] R. Zulkharnay, P. W. May, *J. Mater. Chem. A* **2023**, *11*, 13432.
- [2] M. Syamsul, Y. Kitabayashi, D. Matsumura, T. Saito, Y. Shintani, H. Kawarada, *Appl. Phys. Lett.* **2016**, *109*, 203504.
- [3] S. A. O. Russell, L. Cao, D. Qi, A. Tallaire, K. G. Crawford, A. T. S. Wee, D. A. J. Moran, *Appl. Phys. Lett.* **2013**, *103*, 202112.
- [4] K. G. Crawford, L. Cao, D. Qi, A. Tallaire, E. Limiti, C. Verona, A. T. S. Wee, D. A. J. Moran, *Appl. Phys. Lett.* **2016**, *108*, 042103.
- [5] M. Liao, L. Sang, T. Teraji, S. Koizumi, Y. Koide, *Adv. Mater. Technol.* **2019**, *4*, 1800325.
- [6] J. R. Maze, P. L. Stanwix, J. S. Hodges, S. Hong, J. M. Taylor, P. Cappellaro, L. Jiang, M. V. Gurudev Dutt, E. Togan, A. S. Zibrov, A. Yacoby, R. L. Walsworth, M. D. Lukin, *Nature* **2008**, *455*, 644.
- [7] G. Zhang, T. Samuely, Z. Xu, J. K. Jochum, A. Volodin, S. Zhou, P. W. May, O. Onufriienko, J. Kacmarcik, J. A. Steele, J. Li, J. Vanacken, J. Vacík, P. Szabó, H. Yuan, M. B. J. Roeyfaers, D. Cerbu, P. Samuely, J. Hofkens, V. V. Moshchalkov, *ACS Nano* **2017**, *11*, 5358.
- [8] G. Zhang, T. Samuely, N. Iwahara, J. Kačmarčík, C. Wang, P. W. May, J. K. Jochum, O. Onufriienko, P. Szabó, S. Zhou, P. Samuely, V. V. Moshchalkov, L. Chibotaru, H. Rubahn, *Sci. Adv.* **2020**, *6*, eaaz2536.

- [9] E. A. Ekimov, V. A. Sidorov, E. D. Bauer, N. N. Mel'nik, N. J. Curro, J. D. Thompson, S. M. Stishov, *Nature* **2004**, 428, 542.
- [10] E. Bustarret, *Phys. Stat. Sol. (a)* **2008**, 205, 997.
- [11] E. Bustarret, P. Achatz, B. Sacépé, C. Chapelier, C. Marcenat, L. Ortéga, T. Klein, *Phys. Rev. B* **2007**, 75, 165313.
- [12] E. Bustarret, J. Kacmarcik, C. Marcenat, E. Gheeraert, C. Cytermann, J. Marcus, T. Klein, *Phys. Rev. Lett.* **2004**, 93, 237005.
- [13] G. Zhang, M. Zeleznik, J. Vanacken, P. W. May, V. V. Moshchalkov, *Phys. Rev. Lett.* **2013**, 110, 077001.
- [14] G. Zhang, S. Turner, E. A. Ekimov, J. Vanacken, M. Timmermans, T. Samuely, V. A. Sidorov, S. M. Stishov, Y. Lu, B. Deloof, B. Goderis, G. Van Tendeloo, J. Van de Vondel, V. V. Moshchalkov, *Adv. Mater.* **2014**, 26, 2034.
- [15] G. Zhang, J. Kačmarčík, Z. Wang, R. Zulkharnay, M. Marcin, X. Ke, S. Chiriaev, V. Adashkevich, P. Szabó, Y. Li, P. Samuely, V. V. Moshchalkov, P. W. May, H.-G. Rubahn, *Phys. Rev. Appl.* **2019**, 12, 064042.
- [16] C. D'Errico, S. Scaffidi Abbate, G. Modugno, *Philos. Trans. R. Soc. A* **2017**, 375, 20160425.
- [17] A. Bezryadin, C. N. Lau, M. Tinkham, *Nature* **2000**, 404, 971.
- [18] M. Tinkham, C. N. Lau, *Appl. Phys. Lett.* **2002**, 80, 2946.
- [19] N. Giordano, *Phys. Rev. B* **1990**, 41, 6350.
- [20] W. Zhao, X. Liu, M. H. W. Chan, *Nano Lett.* **2016**, 16, 1173.
- [21] Y. Chen, S. D. Snyder, A. M. Goldman, *Phys. Rev. Lett.* **2009**, 103, 127002.
- [22] F. Altomare, A. M. Chang, M. R. Melloch, Y. Hong, C. W. Tu, *Phys. Rev. Lett.* **2006**, 97, 017001.
- [23] C. Delacour, B. Pannetier, J. Villegier, V. Bouchiat, *Nano Lett.* **2012**, 12, 3501.
- [24] J. N. Voss, Y. Schön, M. Wildermuth, D. Dorer, J. H. Cole, H. Rotzinger, A. V. Ustinov, *ACS Nano* **2021**, 15, 4108.
- [25] A. Ergül, T. Weißl, J. Johansson, J. Lidmar, D. B. Haviland, *Sci. Rep.* **2017**, 7, 11447.
- [26] G. Zhang, R. Zulkharnay, X. Ke, M. Liao, L. Liu, Y. Guo, Y. Li, H. Rubahn, V. V. Moshchalkov, P. W. May, *Adv. Mater.* **2023**, 35, 2211129.
- [27] G. Zhang, T. Samuely, H. Du, Z. Xu, L. Liu, O. Onufriienko, P. W. May, J. Vanacken, P. Szabó, J. Kačmarčík, H. Yuan, P. Samuely, R. E. Dunin-Borkowski, J. Hofkens, V. V. Moshchalkov, *ACS Nano* **2017**, 11, 11746.
- [28] P. Xiong, A. V. Herzog, R. C. Dynes, *Phys. Rev. Lett.* **1997**, 78, 927.
- [29] A. Rogachev, T.-C. Wei, D. Pekker, A. T. Bollinger, P. M. Goldbart, A. Bezryadin, *Phys. Rev. Lett.* **2006**, 97, 137001.
- [30] X. D. A. Baumans, D. Cerbu, O.-A. Adami, V. S. Zharinov, N. Verellen, G. Papari, J. E. Scheerder, G. Zhang, V. V. Moshchalkov, A. V. Silhanek, J. Van de Vondel, *Nat. Commun.* **2016**, 7, 10560.
- [31] S. Michotte, S. Mátéfi-Tempfli, L. Piraux, D. Y. Vodolazov, F. M. Peeters, *Phys. Rev. B* **2004**, 69, 094512.
- [32] D. Y. Vodolazov, *Phys. Rev. B* **2007**, 75, 184517.
- [33] K. Y. Arutyunov, *Phys. C* **2008**, 468, 272.
- [34] D. Y. Vodolazov, F. M. Peeters, *Phys. Rev. B* **2012**, 85, 024508.
- [35] K. Fosshem, A. Sudbø, *Superconductivity: Physics and Applications*, John Wiley & Sons, Hoboken, New Jersey **2004**, pp. 182–183.
- [36] J. Li, M. Ji, T. Schwarz, X. Ke, G. Van Tendeloo, J. Yuan, P. Pereira, Y. Huang, G. Zhang, H. L. Feng, Y. H. Yuan, T. Hatano, R. Kleiner, D. Koelle, L. F. Chibotaru, K. Yamaura, H. B. Wang, P. H. Wu, E. Takayama-Muromachi, J. Vanacken, V. V. Moshchalkov, *Nat. Commun.* **2015**, 6, 7614.
- [37] COMSOL AB, Stockholm, Sweden, Comsol Multiphysics v.5.4.
- [38] J. S. Langer, V. Ambegaokar, *Phys. Rev.* **1967**, 164, 498.
- [39] D. E. McCumber, B. I. Halperin, *Phys. Rev. B* **1970**, 1, 1054.
- [40] N. Giordano, *Physica B: Condens* **1994**, 203, 460.
- [41] A. Bezryadin, *J. Phys.: Condens. Matter* **2008**, 20, 043202.
- [42] O. J. L. Fox, J. O. P. Holloway, G. M. Fuge, P. W. May, M. N. R. Ashfold, *MRS Online Proceedings Library* **2009**, 1203, 1203.